Bioactive Materials 7 (2022) 324–332

Contents lists available at ScienceDirect

Bioactive Materials

journal homepage: www.sciencedirect.com/journal/bioactive-materials

4D biofabrication via instantly generated graded hydrogel scaffolds

Aixiang Ding [a], Sang Jin Lee [a], Sriramya Ayyagari [a], Rui Tang [a], Cong Truc Huynh [a], Eben Alsberg [a,b,*]

[a] Richard and Loan Hill Department of Biomedical Engineering, University of Illinois at Chicago, 909 S. Wolcott Ave., Chicago, IL, 60612, USA
[b] Departments of Mechanical & Industrial Engineering, Orthopaedics, and Pharmacology, University of Illinois at Chicago, 909 S. Wolcott Ave., Chicago, IL, 60612, USA

ARTICLE INFO

Keywords:
Shape-morphing hydrogel
UV absorber
One-step gradient formation
Photolithography
4D bioprinting
Tissue engineering

ABSTRACT

Formation of graded biomaterials to render shape-morphing scaffolds for 4D biofabrication holds great promise in fabrication of complex structures and the recapitulation of critical dynamics for tissue/organ regeneration. Here we describe a facile generation of an adjustable and robust gradient using a single- or multi-material one-step fabrication strategy for 4D biofabrication. By simply photocrosslinking a mixed solution of a photocrosslinkable polymer macromer, photoinitiator (PI), UV absorber and live cells, a cell-laden gradient hydrogel with pre-programmable deformation can be generated. Gradient formation was demonstrated in various polymers including poly(ethylene glycol) (PEG), alginate, and gelatin derivatives using various UV absorbers that present overlap in UV spectrum with that of the PI UV absorbance spectrum. Moreover, this simple and effective method was used as a universal platform to integrate with other hydrogel-engineering techniques such as photomask-aided microfabrication, photo-patterning, ion-transfer printing, and 3D bioprinting to fabricate more advanced cell-laden scaffold structures. Lastly, proof-of-concept 4D tissue engineering was demonstrated in a study of 4D bone-like tissue formation. The strategy's simplicity along with its versatility paves a new way in solving the hurdle of achieving temporal shape changes in cell-laden single-component hydrogel scaffolds and may expedite the development of 4D biofabricated constructs for biological applications.

1. Introduction

Shape-morphing hydrogels that undergo well-defined deformation have been regarded as some of the most promising adaptable materials [1] for a wide range of applications in tissue engineering [2,3], soft-robotic manipulation and locomotion [4], environmental sensing and actuation [5], drug carriers [6], microelectronics [7], and cell scaffolding [8,9]. Particularly, the utilization of shape-morphing hydrogels for 4D biofabrication, referring to the formation of a 3D cell-laden (embedded or seeded) hydrogel bio-construct predesigned to achieve specific geometrical transformation over time [10], is gaining burgeoning momentum because of its potential to enable accurate biomimicry of the functionality and intricate architecture of native tissues/organs [11]. This emerging technology is drawing widespread interest as a strategy to engineer tissues and organs [12]. For example, by seeding cells on the hydrogel surface, Jiang et al. fabricated vascular-mimicking tubular constructs with high precision and tunable sizes using a stress-induced rolling membrane (SIRM) technique [13]. In another example, Zhang et al. developed a 4D physiologically adaptable cardiac patch with seeded cells on the hydrogel surface for the treatment of myocardial infarction [14].

Although there has been substantial progress to date in the field of hydrogel-based 4D biofabrication, there remain limited available cytocompatible materials capable of undergoing 4D transformations in a physiological environment [2]. For 4D hydrogels to support live-cell encapsulation, the materials used must be stringently cytocompatible and the hydrogel fabrication conditions must be mild to ensure high cell viability. To meet these strict requirements, 4D hydrogels have been fabricated using either synthetic or naturally-derived polymers, including poly(ethylene glycol) (PEG) [15], polysaccharides [16], polypeptides [17], and proteins [18] under cell-friendly conditions [19,20]. Furthermore, cytocompatible stimuli such as calcium ions (Ca^{2+}) [21], photoirradiation [22], and hydrogel photo-patterning [23] can be introduced to activate the shape responses in the presence of live cells.

Peer review under responsibility of KeAi Communications Co., Ltd.
* Corresponding author. Richard and Loan Hill Department of Biomedical Engineering, University of Illinois at Chicago, 909 S. Wolcott Ave., Chicago, IL, 60612, USA.
E-mail address: ealsberg@uic.edu (E. Alsberg).

https://doi.org/10.1016/j.bioactmat.2021.05.021
Received 25 March 2021; Received in revised form 5 May 2021; Accepted 6 May 2021
Available online 5 June 2021

Structural and compositional anisotropy can cause uneven swelling and/or shrinking throughout 4D hydrogels and ultimately act to drive the deformation of these shape-morphing constructs [24]. 4D cytocompatible hydrogels with anisotropic swelling have been fabricated with multiple layers or a continuous gradient [11]. For example, Gracias et al. patterned β-TC-6 cell-laden PEG bilayers to form insulin-secretive cylindrical hydrogels [25], Gartner et al. achieved engineered tissue folding by using 3D cell-patterned Matrigel [26], and Ionov et al. fabricated cell-laden ultrathin alginate/hyaluronic acid-based hydrogel films by 3D printing and a subsequent photocrosslinking to produce hollow self-folding tubes [27]. Kasko et al. used photodegradable two-component PEG derivatives to generate a gradient by light-mediated degradation within the hydrogel for dynamic 3D cell culture [28]. While these reports provide valuable insights into the development of 4D biofabricated constructs, they each face limitations with respect to anisotropy generation. For instance, multilayer hydrogel formation typically takes multistep preparation [15] and presents interlayer-adhesion issues [29], ultrathin layer printing substantially limits the geometries and dimensions achievable [27], electrostatic diffusion restricts material options [30], and multiple-component gradient formation exhibits obvious complexity in sample preparation and difficulty in composition control [28]. Therefore, a method to easily and controllably encode the anisotropy into a single-component hydrogel is of high significance.

Previous studies have shown that the incorporation of UV absorber within a preformed photocurable hydrogel can induce effective light decay along the light pathway, resulting in a crosslinking difference in the hydrogel network throughout the hydrogel thickness [31,32]. Similarly, the incorporation of a UV absorber in a photocrosslinkable macromer solution containing a photoinitiator could also effectively bring about a crosslinking gradient during photopolymerization [33–35]. However, these hydrogels were either minimally swelling PEG-derived hydrogels [33,34] or fabricated using non-cytocompatible small molecules [35]. Moreover, the as-prepared hydrogels typically need multiple steps, including a desolvation step by rinsing or volatilization to release the unreacted resins at the low-crosslinking side and a further drying process to generate anisotropic internal strain that induces bending towards the low-crosslinking side. In addition, sudan I, which is broadly regarded as a carcinogen [36], was generally used as the UV absorber in those anisotropic hydrogels formed directly from macromer solutions [30–32]. As such, these systems are not suitable for living cell-related 4D biofabrication studies.

In this work, we demonstrate a simple and versatile approach to generate a tunable and robust gradient in a single-component biocompatible hydrogel for 4D biofabrication through one-step photocrosslinking of a biopolymer solution containing a photoinitiator (PI) and a cytocompatible UV absorber. The instant generation of graded scaffolds was demonstrated using various biocompatible hydrogels, such as those fabricated from 8-arm PEG-acrylate (PEGA8) [37], oxidized and methacrylated alginate (OMA) (Supporting information, and Fig. S1) [38,39], and methacrylated gelatin (GelMA) [40,41]. The tunable crosslinking gradient was easily attained by adjusting fabrication parameters such as polymer concentration, UV absorber concentration, UV irradiation time, and hydrogel thickness, enabling pre-programmable hydrogel deformation. Importantly, multiple cell types (i.e., fibroblasts, stem cells, and cancer cells) were encapsulated into the graded scaffolds with high viability. This simple and cytocompatible strategy permits easy and fast fabrication of cell-laden hydrogel scaffolds with complex structures, which was demonstrated by harnessing several representative techniques, including photomask-aided microfabrication, photomask-based photolithography, ion transfer printing (ITP) [42], and 3D bioprinting. For the proof-of-concept, 4D bone tissue engineering was ultimately explored using this platform system.

2. Materials and methods

2.1. Hydrogel fabrication

A mixed solution of polymer (OMA 6% w/v, GelMA 14% w/v, or PEGA8 20% w/v), PI (0.05% w/v), and UV absorber [methacryloxyethyl thiocarbamoyl rhodamine B (RhB), 4-aminoazobenzene (AAb), fluorescein isothiocyanate derivatives (FITC), and/or 4′-hydroxy-3′-methylacetophenone (HMAP)] in Dulbecco's modified eagle medium-low glucose (DMEM-LG) in the absence/presence of cells (hMSC, NIH3T3, or HeLa, 4×10^6 cells/mL) was placed between two quartz plates with a 0.6 mm spacer and subsequently photocrosslinked with UV light (EXFO OmnicureR S1000, Lumen Dynamics Group) at ~20 mW/cm^2 for varied time to form the hydrogel sheets (OMA 30 s, GelMA 180 s, PEGA8 30 s), which were segmented into hydrogel bars with a dimensions of $13 \times 2 \times 0.6$ (mm × mm × mm). The hydrogel bars were immediately immersed in aqueous solution (specifically defined throughout the Results and Discussion section) to record the corresponding shape changes.

For the bilayer fabrication, OMA hydrogel precursors with or without UV absorber were placed underneath a pre-gelled GelMA layer (formed by 30 s UV crosslinking) and subsequently UV crosslinked for 30 s to form bilayer hydrogels (0.6 mm per layer), which were cut into bilayer bars ($L \times W \times H = 13 \times 2 \times 1.2$, mm × mm × mm) and immersed in water for 30 min at room temperature (RT) to reach maximal bending.

Note that to minimize the potential impact of HMAP on the cell behaviors, culture medium for cell-laden constructs was changed 4 times during the first 2 h (every 30 min) to remove as much of the UV absorber as possible. The details about the definition of bending angle and the angle measurements can be found in the literature [43].

2.2. Reversible shape change study

Hydrogel strips ($13 \times 2 \times 0.6$, mm × mm × mm) fabricated as above (section 2.1, 0.03% w/v RhB, UV 30 s) were cultured in aqueous solutions with varying pH under agitation (Bellco Glass 7744-01010 orbital shaker, Bellco Biotechnology, NJ, USA) at RT to record the shape changes. The agitation speed was set to 2.37 rev/s and incubation solutions were changed every 15 min to record the shapes for each cycle.

2.3. Photomask-aided microfabrication, photo-patterning, ion-transfer printing, and 3D bioprinting

Unless otherwise stated, OMA hydrogel precursor solution was freshly made by dissolving OMA (6% w/v), PI (0.05% w/v) and UV absorber (0.02% w/v HMAP and 0.01% w/v RhB) in DMEM containing hMSCs (4×10^6 cells/mL) for the experiments described below, and all the resulting hydrogels were cultured in cell growth medium (GM) consisting of DMEM, 10% v/v fetal bovine serum (FBS), and 1% v/v penicillin-streptomycin (P/S) in an incubator at 37 °C and 5% CO_2 for 2 h to allow them to fully deform into their final state. The medium was then replaced with PBS (pH 7.4) to take the pictures.

Photomask-aided microfabrication: Hydrogel precursor solution was placed between two quartz plates with spacers (h = 0.4 mm) and covered with a patterned photomask. The solution was exposed to UV light (~20 mW/cm^2) for 30 s. The photomask was removed and the quartz plates were gently separated, the microfabricated hydrogels attached on the surface of both plates were gently flushed into wells of a 6-well plate (Corning, NY, USA) using GM, and a total volume of 5 mL medium was used for hydrogel culture in each well.

Photo-patterning: Hydrogel precursor solution was placed between two quartz plates separated with spacers (h = 0.6 mm) and then exposed to UV light for 30 s to form the hydrogels. Subsequently, a stripe-patterned photomask (stripe width 0.2 mm) was placed over the top plate, and UV light was further applied to crosslink for 60 s. The hydrogels were tailored using a punch into squares (sheet, 19 × 19, mm

× mm) or circles (disk, $d = 20$ mm), which were immersed in 5 mL of GM in 6-well plate wells for culture. Non-patterned hydrogel sheets (19 × 19, mm × mm) and disks ($d = 20$ mm) were fabricated under UV irradiation for different times (40, 60, and 80 s) without patterning and then cultured to afford 3D cell-laden constructs with varying curvatures for comparison.

Ion-transfer printing: Hydrogels formed as above (Section 2.1, UV 30 s) were cut into hydrogel bars (14 × 20 × 0.6, mm × mm × mm) or hydrogel squares (20 × 20 × 0.6, mm × mm × mm). Then these tailored hydrogel constructs were covered by a filter paper with a specific pattern for 30 s. Note that the filter paper was pre-soaked in calcium chloride (1 M) solution for 5 min. Then, the post-treated hydrogels were immersed in 5 mL of GM medium in wells of a 6-well plate for culture.

4D bioprinting: Hydrogel precursor solution was loaded into a 1 mL syringe with a 0.5-inch 30G stainless steel needle (McMaster-Carr) and printed using a 3D printer (PrintrBot SimpleMetal 3D Printer, Printrbot). More details about this printer can be found in the literature [44]. Digital models for 3D printing were generated from www.tinkercad.com. An empty Petri dish was placed on the building platform. The tip of the needle was positioned at the center and near the bottom of the dish, and the print instructions were sent to the printer using the host software (Cura Software, Ultimaker), which is an open source 3D printer host software [38]. The printed hydrogel precursor solution was imaged and immediately subjected to photocrosslinking (UV 30 s at ~20 mW/cm^2 intensity). Then, the hydrogel construct was gently transferred into a well of a 6-well plate filled with 5 mL of GM, cultured under the same conditions as above for 30 min, and imaged.

3. Results and Discussion

A typical setup and the process for the fast fabrication of graded hydrogel scaffolds is schematically illustrated in Fig. 1a and b. Photocurable polymer was first dissolved in DMEM containing both PI and UV absorber (DMEM was used as solvent to promote subsequent viability of encapsulated cells) to form the hydrogel precursor solution, which was then placed between two quartz plates located at an adjustable distance from a UV light source. Since photo-curing efficiency relies on the irradiation intensity that the PI receives, and the irradiation intensity decays more rapidly with distance along the light travelling pathway with the co-existence of UV absorber, a gradient in crosslinking density can be readily generated with the top portion of the hydrogel closest to the light source showing high crosslinking density while the bottom portion is crosslinked to the lowest extent. This hydrogel bearing the crosslinking gradient can be further tailored into specifically shaped hydrogels and directly cultured in a medium to initiate deformation (Fig. 1b). It is noteworthy that it is the subsequent anisotropic swelling induced internal strain that causes the deformation towards the high-crosslinking side herein, which is different from deformations resulting from the generated anisotropic internal strain during the desolvation step that causes deformation towards the low-crosslinking side in previously reported gradient hydrogels [33–35].

To examine the versatility of this approach, synthetic polymer PEGA8, natural polysaccharide-derivatived OMA, and natural protein-derivatived GelMA were employed as biocompatible polymers, and a fluorescence dye RhB with an effective overlap in the UV absorption spectrum with the PI was selected as a UV absorber (Fig. S2a). Hydrogels were prepared and incubated in water for 4 h to ensure equilibrated swelling (see details in Supporting Information). As shown in Fig. 1c-e, hydrogels that were fabricated in the presence of RhB exhibited evident bending, while those hydrogels formed without RhB incorporation in the precursor solution exhibited almost no or only slight bending (Fig. S3). It should be noted that although photocrosslinked PEGDA

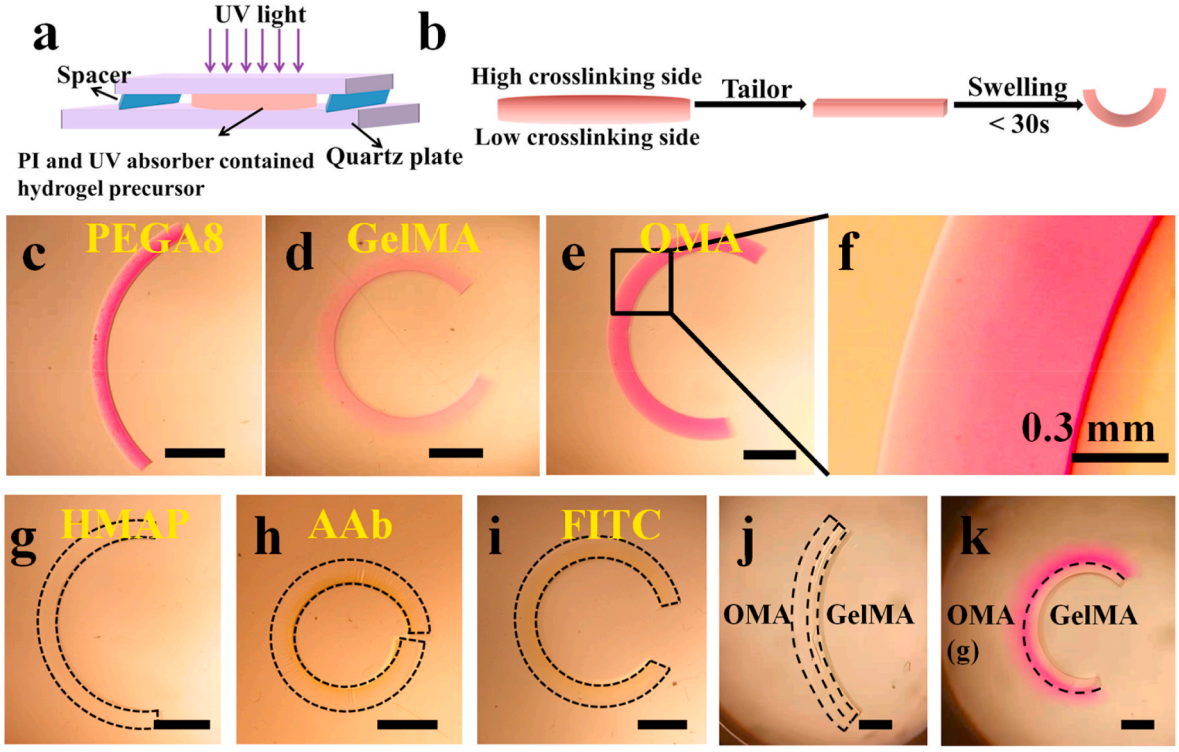

Fig. 1. (a) A typical setup for crosslinking gradient hydrogel fabrication; (b) Schematic showing gradient hydrogel cut into specific initial shape and its subsequent deformation after swelling; Curved hydrogel bars of (c) PEGDA, (d) GelMA, and (e) OMA obtained using RhB (0.03% w/v) as UV absorber; (f) Magnified image showing a clear continuous gradient in the OMA hydrogel; Curved hydrogel bars of OMA obtained using (g) FITC (0.03% w/v), (h) AAb (0.05% w/v), and (i) HMAP (0.01% w/v) as UV absorber; bilayer hydrogel bars obtained from (j) OMA/GelMA and (k) OMA(g)/GelMA demonstrating feasibility of multi-material fabrication, where OMA represents non-gradient OMA hydrogel and OMA(g) represents gradient OMA hydrogel. The dotted outlines indicate (g–j) the shape of the hydrogel bars or (j–k) the interface of two layers. Scale bars in c-e and g-k indicate 2 mm.

hydrogels typically do not swell much in medium [33] and no deformation was shown in previous PEGDA hydrogels during rinsing [33,34], a clearly discernible bending was observed in the present case, which can likely be ascribed to the large difference in crosslinking density across the height of the construct.

There are other common compounds in addition to RhB that possess some overlap in UV absorbance spectrum with that of PI, such as colorless HMAP, the non-fluorescent dye AAb, and FITC (Fig. S2b-d), and can be used as UV absorbers. Similarly, rapid hydrogel bending was also clearly observed with these three additional examples (Fig. 1g-i), indicating the effectiveness of crosslinking gradient formation caused by the attenuated UV absorption from the hydrogel surface that first receives light to the surface furthest from the source [28] due to use of these UV absorbers [45]. Importantly, the UV absorber plays a critical role in the attenuation of UV light absorption in this system. In OMA hydrogels, for example, RhB or HMAP incorporation preserved substantially more methacrylate groups compared with the hydrogel lacking a UV absorber (Fig. S4), with the amount of methacrylate groups remaining after UV crosslinking reflecting the extent of the photo-induced reaction. The continuous nature of the formed gradient was directly visualized in RhB incorporated hydrogels at higher magnification (Fig. 1f and Fig. S5).

Although single material fabrication is straightforward, some application may benefit from or even require a multi-material system. In addition to single material fabrication, this strategy also applies to multi-material fabrication in a single step. To demonstrate this, bilayer hydrogels comprised of one gradient OMA [OMA(g)] layer and one GelMA layer, referred to as OMA(g)/GelMA, were fabricated (Fig. S6a). The key difference for the bilayer fabrication lies in the use of a hydrogel layer containing crosslinkable methacrylates on the surface that directly covers the OMA hydrogel precursor solution so that a strong interfacial adhesion can be formed after UV crosslinking. For comparison, bilayers that consist of non-gradient OMA and GelMA hydrogels (OMA/GelMA) were also fabricated. After reaching equilibrium swelling in water, OMA (g)/GelMA bent to a much larger extent than OMA/GelMA, due to the remarkably enhanced deformation ability of the gradient layer (Fig. 1j, k, and Fig.S6b), implying that the integration of a gradient layer into a multi-material system can be an effective way to alter or improve the deformability.

The effects of important parameters including UV irradiation time, UV absorber concentration, hydrogel thickness, polymer concentration, and swelling medium on construct morphing behavior were comprehensively investigated using OMA hydrogel bars as a prototype. Since the extent of crosslinking gradient differential across the hydrogel bar thickness strongly affects the bending angle, those parameters with the greatest capacity to augment the crosslinking gradient such as decreased UV exposure time (Fig. 2a), increased RhB concentration (Fig. 2b), and increased hydrogel thickness (<0.8 mm, Fig. 2c) resulted in a larger bending. Interestingly, while it is usually observed that increasing hydrogel bar thickness decreases its bending degree [42,46,47], the opposite phenomenon was observed in our case. However, the bending extent decreased again when the thickness reached 1.0 mm. It should be noted that, in the above hydrogels, in addition to the augmented gradient range, increased volumetric swelling caused by lowered overall crosslinking density (Fig. S7) also contributed to the increased bending. Moreover, polymer concentration and choice of aqueous swelling solution also exerted clear influence on the hydrogel bending. Hydrogels prepared at a concentration of 6% (w/v) and immersed in the H_2O displayed maximum bending (Fig. 2d and e). The increase in the polymer concentration not only augments the gradient range but also diminishes hydrogel swelling at the same time (Fig. S8a). The final bending result stems from the competition of these two factors. The hydrogel swelling findings in different aqueous solutions, in contrast, is consistent with those of hydrogel deformation, in that higher swelling gave rise to increased bending (Fig. S8b). Thus, it can be seen that the bending degree can be finely tuned by altering any of these parameters, including the formulation of the hydrogel precursor solution, hydrogel dimensions, as well as culture medium. The parameters were set at 6% polymer concentration, 30 s UV irradiation, and 0.6 mm thickness for the following experiments unless stated otherwise.

The implementation of tunability of the deformation extent after hydrogel fabrication by treatment post-fabrication offers a second powerful opportunity to modulate the hydrogel geometry. Given that swelling of alginate-derived hydrogels can be modulated by both the incubation solution pH [48] and divalent cation chelators such as ethylenediaminetetraacetic acid (EDTA), a strong Ca^{2+} chelating agent

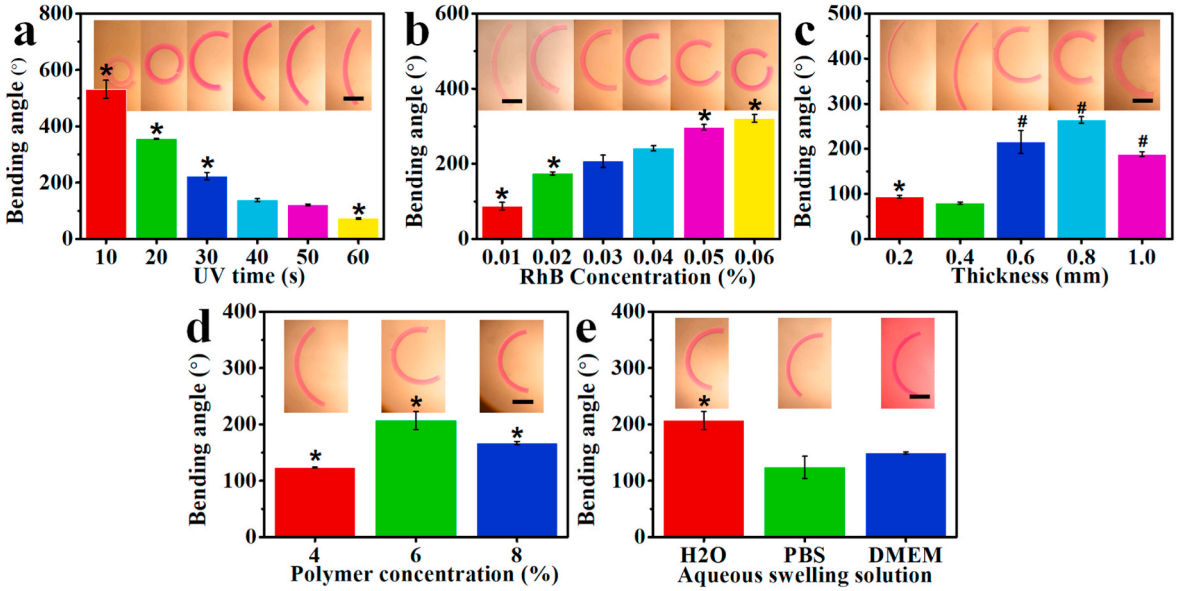

Fig. 2. Bending degree of OMA hydrogels as a function of (a) UV irradiation time (6% w/v polymer, 0.6 mm thickness, 0.03% w/v RhB) in H_2O, $^*p < 0.05$ compared with all other groups, (b) RhB concentration (6% w/v polymer, 0.6 mm thickness, 30 s UV) in H_2O, $^*p < 0.05$ compared with all other groups, (c) hydrogel thickness (6% w/v polymer, 0.03% w/v RhB, 30 s UV) in H_2O, $^*p < 0.05$ compared with all other groups except for "0.4", $^{\#}p < 0.05$ compared with all other groups, (d) polymer concentration (0.6 mm thickness, 0.03% w/v RhB, 30 s UV) in H_2O, $^*p < 0.05$ compared with all other groups, and (e) aqueous swelling solution (6% w/v polymer, 0.6 mm thickness, 0.03% w/v RhB, and 30 s UV), $^*p < 0.05$ compared with all other groups. All scale bars indicate 2 mm.

with the ability to snatch Ca^{2+} from the alginate network [49], the shape controllability of hydrogels post-fabrication was then demonstrated using the stimuli-responsive OMA hydrogels as an example. By soaking the hydrogel bars in water solutions of pH 1 or 7 or water solutions containing Ca^{2+} or EDTA, they showed reversible shrinkage and swelling (insets of Fig. 3a and b), which in turn brought about changes in the hydrogel bending. When repeatedly switching the solutions (Fig. 3a and b), the hydrogels repeatedly recovered their previous shape after the first deformation cycle. These findings demonstrate the capacity to adjust the shape of these constructs on demand.

Owing to biocompatibility of the materials and friendliness of the fabrication process towards the cells, encapsulation of cells within the hydrogels was examined. Cell-laden hydrogel bars were fabricated under the same conditions as described earlier and then cultured in the GM to investigate both the role of cells in construct shape change and cell viability in the system. Specifically, three cell types were examined: human mesenchymal stem cell (hMSC), a fibroblast cell line (NIH3T3), and a cervical cancer cell line (HeLa). In addition, HMAP (0.02%) was used as UV absorber due to its high efficiency for gradient generation, noninterference with the live/dead cell staining assay, and high cytocompatibility (Fig. S9, >90% cell viability in all the tested concentrations). Cell-laden hydrogel bars exhibited larger extent of bending compared to those without cells (Fig. 3c). This may be a result of the cells weakening light penetration by absorption, reflection, and scattering in the hydrogels. Nonetheless, non-gradient cell-laden hydrogel bars with cell density up to 1×10^8 cells/mL hydrogel precursor solution displayed no obvious bending (Fig. S10), suggesting the essential contribution of the effective gradient formation in driving the shape changes of the cell-laden constructs. All the three types of embedded cells maintained predominantly round morphology (Fig. S11) and high average viability after 3 days culture (~86%–89%, Fig. 3d), albeit slightly lower than the control group (UV absorber-free group, ~90%–96% viability, Fig. 3d and Fig. S12). These results indicate that the dilemma of live-cell encapsulation in the shape-morphing hydrogels, which is deemed as a current challenge in the 4D biofabrication field [11], can be easily overcome using this one-step gradient-generation strategy.

Taking advantage of this platform system's simplicity and biocompatibility, the utility of applying additional hydrogel-engineering techniques, such as photo-aided microfabrication, photo-patterning, ITP, and 3D bioprinting, to fabricate cell-laden OMA hydrogel scaffolds with more sophisticated structures was investigated. To aid in visualization of the constructs, a combination of 0.02% RhB and 0.01% HMAP was used as a mixed UV absorber.

First, a photomask-aided 4D bio-microfabrication process (Fig. S13a) was developed for rapid manufacture of large-scale bio-microstructures. For example, multiple cell-laden six-petal micro-blossoms (Fig. 4a_1) and four-arm micro-grippers (Fig. 4a_2) can be produced from a single batch. Samples with larger sizes using the same method were also made (Fig. S13b). Compared with the fabrication of shape-morphing micro-multilayers using photomask-based multistep photocrosslinking [25] or micro-molding approaches [50], which either needs accurate alignment or long-time preparation, regardless of biocompatibility, this one-step 4D biofabrication strategy on a whole is much simpler, faster and more economical. These bio-microstructures might in the future be expanded to be applied as bio-microactuators if a stimuli-responsiveness is integrated [51]. Based on the gradient crosslinking principle, multiple-gradients can be intentionally produced with more than one direction in a single hydrogel construct. For example, a single hydrogel bar with a "double-faced" gradient (Fig. 4b_1) was fabricated by simply controlling the photomask and UV irradiation direction (Fig. S14). This bi-gradient hydrogel bar deformed into an "*S*" shape after swelling (Fig. 4b_2). Therefore, using this technique, it is easy to generate more complex structures with dissymmetric geometries in a single-layer hydrogel.

Next, photo-patterning of prefabricated gradient hydrogels was conducted using a mask-based photolithography technique to yield cell-laden macroscopic 3D structures (Fig. S15a). The post-patterning of the hydrogels enables patterning multiple user-defined regions to induce specific 4D architectural shape conversions [52]. Pre-fabricated cell-laden gradient hydrogel sheets or disks were covered with a patterned photomask and then transferred to the GM for saturating at least 2 h at 37 °C. Then clear images of deformed hydrogels were taken after replacing the GM with PBS. It was observed that the hydrogel sheets formed under photomasks with parallel strips (Fig. 4c_1) curled up into well-shaped hydrogel tubes (Fig. 4c_2 and 4c_3). Similarly, disk-shape-based hydrogel tubes were also obtained (Fig. S15b). Interestingly, by changing the patterned parallel strips into inclined strips, hydrogel sheets curled up into misaligned hydrogel tubes through diagonal rolling (Fig. S15c). Even though large cell-laden constructs with well-defined 3D structures, such as curled hydrogels with

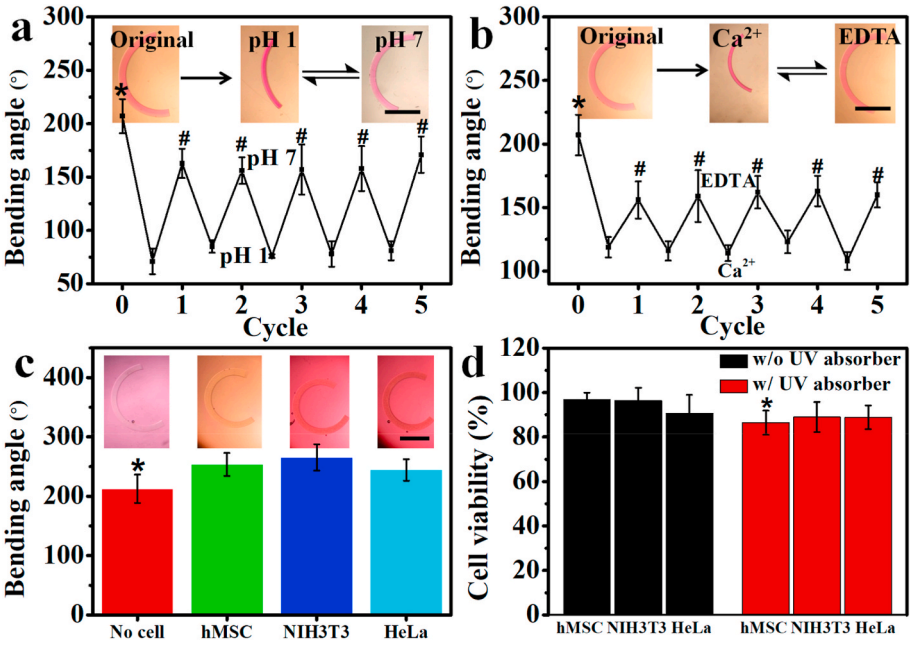

Fig. 3. Cyclic reversible bending angle of OMA hydrogel bars in water solutions (a) of alternating pH of 1 and 7 and (b) with alternating presence of chemicals EDTA and Ca^{2+}, 0.03% w/v RhB, $^*p < 0.05$ compared with all other groups, $^\#p < 0.05$ compared with "pH 1" and original groups, scale bars indicate 4 mm. (c) Bending degree of cell-free and cell-laden OMA hydrogel bars in GM, 0.02% w/v HMAP, $^*p < 0.05$ compared with all other groups, scale bars indicate 2 mm. (d) Viability of encapsulated cells inside non-gradient (without UV absorber) and gradient (with UV absorber) hydrogels in GM after 3 days culture, 0.02% w/v HMAP, $^*p < 0.05$ compared to hMSC without UV absorber group. Insets: representative images showing the deformed shapes under respective conditions.

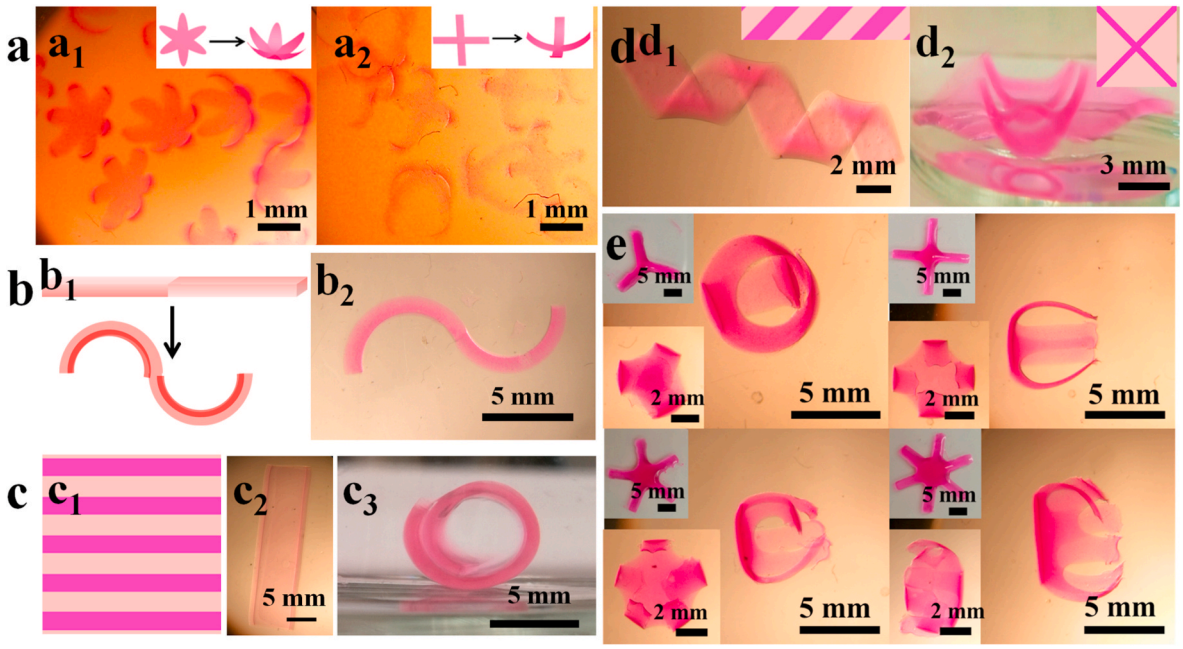

Fig. 4. Images of 4D biofabricated cell-laden structures: (a_1) six-petal blossoms and (a_2) four-arm grippers obtained by photomask-aided biofabrication, insets illustrate the deformation process of the microfabricated hydrogels; (b_1) Schematic of a "double-faced" hydrogel bar and its deformation, and (b_2) a typical "*S*" shape formed by the "double-faced" hydrogel; (c) hydrogel tubes obtained by post-photopatterning of a pre-fabricated gradient hydrogel sheet or disk, (c_1) patterned regions on a hydrogel sheet with dark pink regions denoting the UV-exposed section, (c_2) top-view image obtained using an optical microscope, (c_3) side-view image taken in ambient light; ITP-generated (d_1) hydrogel spiral and (d_2) pseudo-four-petal flower, insets show the ion-printed section on a pre-formed gradient hydrogel bar or hydrogel sheet; and (e) bioprinted multiple-arm grippers and their deformed structures, insets show the as-printed hydrogel construct before photo-gelation (upper left) and the top view of deformed hydrogel constructs (lower left). All hydrogel deformations were performed in GM at 37 °C for at least 2 h to obtain ultimate stable structures, and images were taken after replacing the GM with PBS (pH 7.4) for clarity.

varying curvatures, can be easily obtained by rolling of those hydrogel sheets and disks fabricated with different UV irradiation times (Fig. S16), the photo-patterning technique could endow hydrogels with larger deformations and greater curvature [e.g., patterned hydrogels with 60 s UV irradiation (Fig. 3c and Fig. S15)] and with more abundant structures [e.g., misaligned tube formation (Fig. S15c)] than those formed from non-patterned hydrogel sheets with the same or even lower UV irradiation time (Fig. S16).

In addition to the above photolithographic techniques, an ITP strategy [42] was introduced to locally treat the pre-formed gradient hydrogel with Ca^{2+} to locally induce secondary ionic crosslinking to the OMA hydrogel (Fig. S17), causing constrained local swelling [30]. By printing these divalent cations on specific regions of cell-laden hydrogel bars or hydrogel sheets (insets in Fig. 4d, dark pink section denotes cation-printed section), cell-laden spirals (Fig. 4d_1) and cell-laden pseudo-four-petal followers (Fig. 4d_2) were obtained.

Finally, this platform strategy was integrated into the realm of 4D bioprinting, a state of the art biofabrication technology that incorporates time-dependence into 3D bioprinting to confer conformational changes to printed biosamples, which may enable recapitulation of dynamic tissue and organ geometric evolution that occurs during development and regeneration [53]. A cell-laden hydrogel bar was first printed and photocrosslinked to verify the feasibility of 4D bioprinting. As expected, this hydrogel bar folded into a hydrogel ring after being immersed in GM (Fig. S18a). Next, various cell-laden multiple-arm grippers were printed (Fig. S18b and insets on the upper left of Fig. 4e), photocrosslinked, and cultured to permit respective structural deformation to occur (Fig. 4e). Importantly, all these techniques do not compromise cell viability. To exclude the influence of RhB on live/dead cell staining visualization, parallel experiments under the same conditions were performed with HMAP (0.02% w/v) as the sole UV absorber to assess cytocompatibility. hMSCs within these 4D fabricated hydrogels were highly viable after 3 days culture, as indicated by the live/dead staining results (Fig. S19). Thus, this 4D biofabrication approach is compatible with other live-cell encapsulation techniques, making it useful for biomedical engineering applications.

4D biofabricated scaffolds capable of undergoing dynamic shape transformations may enable the engineering of tissues with complex geometries and replication of critical morphodynamic evolutions that occur during native tissue development [43,54]. Design of conventional inductive hydrogel scaffolds for tissue engineering that are geometrically static often primarily focuses on controlling microenvironmental physiochemical niches for guiding cell behavior and new tissue formation and generally neglects important macroscopic morphing. The potential to differentiate stem cells within this 4D biofabrication platform for 4D tissue engineering applications was thus explored. A 4D osteogenesis study was conducted as a proof-of-concept by culturing an hMSC-laden hydrogel bar in the osteogenic medium over a course of four weeks, during which time its shape was continuously monitored. Cell viability, DNA content, and osteogenic markers such as alkaline phosphates (ALP) activity and calcium deposition were examined to evaluate the extent of osteogenic differentiation. Similar to findings after culturing in the GM, these hydrogel bars rapidly curled into an opened ring (<3 min) and then remained almost unchanged in shape during the 4-week culture (Fig. 5a), demonstrating robust geometrical stability. The live/dead staining results also revealed high cell viability after 4-week culture (Fig. 5b). For the osteogenesis study, hydrogel bars serving as the negative control (NC) were fabricated the same as those of the experimental group (EG), but they were cultured in the GM. Hydrogel bars serving as the positive control (PC) were prepared without incorporation of a UV absorber and cultured in osteogenic medium. The DNA levels were relatively constant over the entire culturing period (Fig. 5c), whereas the ALP activity and calcium content (both normalized to DNA) in the EG and PC significantly increased over time (except for ALP/DNA within the EG group from W1 to W2) and were significantly higher than those of NC. There was no significant

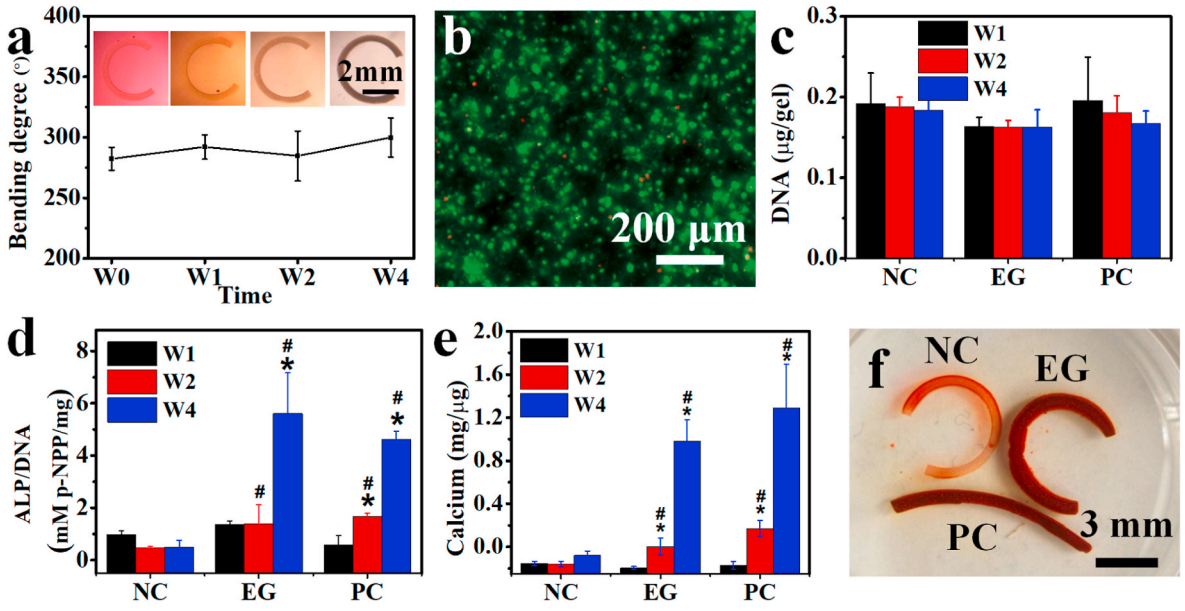

Fig. 5. (a) Bending degree of cell-laden hydrogel bars as a function of culture time in osteogenic medium. Inset: representative images at respective time points showing the shapes of the cell-laden hydrogel bars. (b) Live/dead staining images of encapsulated cells inside a hydrogel bar after 4-week culture in osteogenic medium. Biochemical quantification of (c) DNA content, (d) ALP activity normalized to DNA content, and (e) calcium content normalized to DNA content in the cell-laden hydrogels at varying time points. NC (negative control): cell-laden hydrogel bar obtained in the presence of UV absorber and cultured in GM, EG (experimental group): cell-laden hydrogel bar obtained in the presence of UV absorber and cultured in osteogenic medium, PC (positive control): cell-laden hydrogel bar obtained in the absence of UV absorber and cultured in osteogenic medium. (f) Typical alizarin red stained cell-laden hydrogel bars after 4-week culture. $^{*}p < 0.05$ compared with all other time points within a group, $^{\#}p < 0.05$ compared with NC group at the same time point.

difference found between the EG and PC at any time point (Fig. 5d and e). The calcium content, a critical component of hydroxyapatite formation during osteogenesis, in EG and PC hydrogel bars was confirmed by dark alizarin red staining throughout the constructs (Fig. 5f). These results support the conclusion that the hydrogel deformation and cell differentiation within the hydrogel are generally independent of each other in this system, and thus they can be designed separately.

Morphological change is a common phenomenon that occurs during tissue maturation [55]. Compared with 3D scaffolds, 4D scaffolds with the ability to reconfigure their shapes during culture show huge potential for morphodynamic tissue engineering. Hydrogels that harness non-uniform swelling [43,54,56–58], post-programmed anisotropic internal strains [59,60], or cell contractile forces [61–63] can accomplish this task. However, in addition to the stringent requirements regarding material cytocompatibility, the fabrication process, and imposed stimulation, complexity in fabrication and lack of controllability present a significant impedance to 4D tissue engineering. 4D biofabrication using a simple, cost-effective, and robust one-step photocrosslinking method to generate instantly applicable scaffolds may help to realize the potential of 4D strategies in tissue engineering, as clearly demonstrated by our 4D bone-like tissue engineering study. It is interesting to note we did not observe a difference between the PC and EG groups (Fig. 5). One plausible reason is that there was negligible difference in the response of the encapsulated cells to the internal strain within the straight hydrogel slabs compared to the anisotropic internal strain distribution within the curved hydrogel slabs. In the future, using different mechanically sensitive cells (e.g., cardiomyocytes) or further increasing the structural anisotropy and internal strain represent possible ways to examine the impact of the 4D process on cell behaviors. Nevertheless, additional engineering of the materials, such as modification with cell adhesive ligands (e.g., RGD peptide motif) [64–66], tuning matrix physical properties [67], facilitation of cell-cell interactions [54] and/or controlled delivery of bioactive factors [68–71], may also be further explored to promote survival of diverse encapsulated cell population and enhance cell functioning.

4. Conclusion

4D biofabrication for biomedical applications requires not only effective anisotropy formation but also often necessitates conditions that facilitate cell encapsulation and long-term viability. A simple and efficient strategy comprised of only one-step photocrosslinking of cell-containing hydrogel precursor solution was engineered to achieve this goal. This study demonstrates a versatile technology in which the incorporation of UV absorber directly into the photocrosslinkable biopolymer solution creates an adjustable gradient, allowing for on-demand, controllable and cytocompatible hydrogel shape remodeling. This approach also exhibited enormous tolerance and adaptability, where not only diverse polymers and UV absorbers can be used as needed but also the strategy itself can be effectively integrated with other hydrogel-engineering techniques or platforms. In this manner, a facile and straightforward path has been established for concurrently enabling controllable, time-dependent shape changes into biomaterials along with encapsulated living cells, which has great potential in 4D biofabrication for biomedical applications such as biosensing and bioactuation in living systems and tissue engineering.

CRediT authorship contribution statement

Aixiang Ding: Conceptualization, Material synthesis, Methodology, Validation, Formal analysis, Data curation, Writing – original draft, Visualization. **Sang Jin Lee:** Methodology, Formal analysis. **Sriramya Ayyagari:** Methodology, Formal analysis. **Rui Tang:** Methodology, Writing – review & editing. **Cong Truc Huynh:** Material synthesis. **Eben Alsberg:** Conceptualization, Methodology, Formal analysis, Resources, Supervision, Funding acquisition, Writing – review & editing.

Declaration of competing interest

The authors declare that they have no known competing financial interests or personal relationships that could have appeared to influence the work reported in this paper.

Acknowledgements

The authors gratefully acknowledge funding from the National Institutes of Health's National Institute of Arthritis and Musculoskeletal and Skin Diseases (R01AR069564, and R01AR066193; E.A.), National Institute of Biomedical Imaging and Bioengineering (R01EB023907; E. A.), and National Heart, Lung, and Blood Institute (T32HL007829; R.T.). The contents of this publication are solely the responsibility of the authors and do not necessarily represent the official views of the National Institutes of Health. The authors also thank Susan R. Ross at University of Illinois at Chicago for generously providing the NIH3T3 cells.

Appendix A. Supplementary data

Supplementary data to this article can be found online at https://doi.org/10.1016/j.bioactmat.2021.05.021.

References

[1] S.-J. Jeon, A.W. Hauser, R.C. Hayward, Shape-morphing materials from stimuli-responsive hydrogel hybrids, Acc. Chem. Res. 50 (2) (2017) 161–169.
[2] S. Miao, N. Castro, M. Nowicki, L. Xia, H. Cui, X. Zhou, W. Zhu, S.-j. Lee, K. Sarkar, G. Vozzi, Y. Tabata, J. Fisher, L.G. Zhang, 4D printing of polymeric materials for tissue and organ regeneration, Mater, Today 20(10) (2017) 577–591.
[3] N. Liu, X. Ye, B. Yao, M. Zhao, P. Wu, G. Liu, D. Zhuang, H. Jiang, X. Chen, Y. He, S. Huang, P. Zhu, Advances in 3D bioprinting technology for cardiac tissue engineering and regeneration, Bioact. Mater 6 (5) (2021) 1388–1401.
[4] D. Han, C. Farino, C. Yang, T. Scott, D. Browe, W. Choi, J.W. Freeman, H. Lee, Soft robotic manipulation and locomotion with a 3D printed electroactive hydrogel, ACS Appl. Mater. Interfaces (2018) 17512–17518, 10(21).
[5] S. Li, K.W. Wang, Plant-inspired adaptive structures and materials for morphing and actuation: a review, Bioinspiration Biomimetics 12 (1) (2016) 11001.
[6] S. Fusco, H.-W. Huang, K.E. Peyer, C. Peters, M. Häberli, A. Ulbers, A. Spyrogianni, E. Pellicer, J. Sort, S.E. Pratsinis, B.J. Nelson, M.S. Sakar, S. Pané, Shape-switching microrobots for medical applications: the influence of shape in drug delivery and locomotion, ACS Appl. Mater. Interfaces (2015) 6803–6811, 7(12).
[7] X. Du, H. Cui, B. Sun, J. Wang, Q. Zhao, K. Xia, T. Wu, M.S. Humayun, Photothermally triggered shape-adaptable 3D flexible electronics, Adv. Mater. Technol 2 (10) (2017) 1700120.
[8] Q. Zhao, J. Wang, H. Cui, H. Chen, Y. Wang, X. Du, Programmed shape-morphing scaffolds enabling facile 3D endothelialization, Adv. Funct. Mater. 28 (29) (2018) 1801027.
[9] M.P. Nikolova, M.S. Chavali, Recent advances in biomaterials for 3D scaffolds: a review, Bioact, Mater 4 (2019) 271–292.
[10] X. Zhu, H. Yang, 4D Biofabrication of branching multicellular structures: a morphogenesis simulation based on turing's reaction-diffusion dynamics, IOP Conf. Ser, Mater. Sci. Eng. 280 (2017) 12018.
[11] L. Ionov, 4D biofabrication: materials, methods, and applications, Adv. Healthcare Mater 7 (17) (2018) 1800412.
[12] G.H. Yang, M. Yeo, Y.W. Koo, G.H. Kim, 4D bioprinting: technological advances in biofabrication, Macromol. Biosci. 19 (5) (2019) 1800441.
[13] B. Yuan, Y. Jin, Y. Sun, D. Wang, J. Sun, Z. Wang, W. Zhang, X. Jiang, A strategy for depositing different types of cells in three dimensions to mimic tubular structures in tissues, Adv, Mater 24 (7) (2012) 890–896.
[14] H. Cui, C. Liu, T. Esworthy, Y. Huang, Z.-x. Yu, X. Zhou, H. San, S.-j. Lee, S.Y. Hann, M. Boehm, 4D physiologically adaptable cardiac patch: a 4-month in vivo study for the treatment of myocardial infarction,, Sci. Adv 6 (26) (2020) eabb5067.
[15] H.R. Kwag, J.V. Serbo, P. Korangath, S. Sukumar, L.H. Romer, D.H. Gracias, A self-folding hydrogel in vitro model for ductal carcinoma, Tissue Eng. Part C: Methods 22(4) (2016) 398–407.
[16] Y. Luo, X. Lin, B. Chen, X. Wei, Cell-laden four-dimensional bioprinting using near-infrared-triggered shape-morphing alginate/polydopamine bioinks, Biofabrication 11 (4) (2019) 45019.
[17] M.A. Gonzalez, J.R. Simon, A. Ghoorchian, Z. Scholl, S. Lin, M. Rubinstein, P. Marszalek, A. Chilkoti, G.P. López, X. Zhao, Strong, tough, stretchable, and self-adhesive hydrogels from intrinsically unstructured proteins, Adv. Mater. 29 (10) (2017) 1604743.
[18] Y.S. Zhang, A. Khademhosseini, Advances in engineering hydrogels, Science 356 (6337) (2017) eaaf3627.
[19] C. Löwenberg, M. Balk, C. Wischke, M. Behl, A. Lendlein, Shape-memory hydrogels: evolution of structural principles to enable shape switching of hydrophilic polymer networks, Acc. Chem. Res. 50 (4) (2017) 723–732.
[20] M.A. Heinrich, W. Liu, A. Jimenez, J. Yang, A. Akpek, X. Liu, Q. Pi, X. Mu, N. Hu, R. M. Schiffelers, 3D bioprinting: from benches to translational applications, Small 15 (23) (2019) 1805510.
[21] X. Du, H. Cui, Q. Zhao, J. Wang, H. Chen, Y. Wang, Inside-out 3D reversible ion-triggered shape-morphing hydrogels, Research 2019 (2019) 6398296.
[22] F. Pilate, A. Toncheva, P. Dubois, J.-M. Raquez, Shape-memory polymers for multiple applications in the materials world, Eur. Polym. J. 80 (2016) 268–294.
[23] J. Bai, Z. Shi, Shape memory: an efficient method to develop the latent photopatterned morphology for elastomer in two/three dimension, ACS Macro Lett. 6 (9) (2017) 1025–1030.
[24] K. Sano, Y. Ishida, T. Aida, Synthesis of anisotropic hydrogels and their applications, Ang. Chem. Int. 57 (10) (2018) 2532–2543.
[25] M. Jamal, S.S. Kadam, R. Xiao, F. Jivan, T.M. Onn, R. Fernandes, T.D. Nguyen, D. H. Gracias, Bio-origami hydrogel scaffolds composed of photocrosslinked PEG bilayers, Adv. Healthcare Mater 2 (8) (2013) 1142–1150.
[26] A.J. Hughes, H. Miyazaki, M.C. Coyle, J. Zhang, M.T. Laurie, D. Chu, Z. Vavrušová, R.A. Schneider, O.D. Klein, Z.J. Gartner, Engineered tissue folding by mechanical compaction of the mesenchyme, Dev. Cell (2018) 165–178, 44(2), e6.
[27] A. Kirillova, R. Maxson, G. Stoychev, C.T. Gomillion, L. Ionov, 4D biofabrication using shape-morphing hydrogels, Adv. Mater. 29 (46) (2017) 1703443.
[28] E. Käpylä, S.M. Delgado, A.M. Kasko, Shape-changing photodegradable hydrogels for dynamic 3D cell culture, ACS Appl. Mater. Interfaces (2016) 17885–17893, 8 (28).
[29] D. Jin, Q. Chen, T.-Y. Huang, J. Huang, L. Zhang, H. Duan, Four-dimensional direct laser writing of reconfigurable compound micromachines, Mater. Today 32 (2020) 19–25.
[30] H. Cui, N. Pan, W. Fan, C. Liu, Y. Li, Y. Xia, K. Sui, Ultrafast fabrication of gradient nanoporous all-polysaccharide films as strong, superfast, and multiresponsive actuators, Adv. Funct. Mater. 29 (20) (2019) 1807692.
[31] C.-M. Chen, J.C. Reed, S. Yang, Guided wrinkling in swollen, pre-patterned photoresist thin films with a crosslinking gradient, Soft Matter (2013) 11007–11013, 9(46).
[32] Y. Zhou, C.M. Duque, C.D. Santangelo, R.C. Hayward, Biasing buckling direction in shape-programmable hydrogel sheets with through-thickness gradients, Adv. Funct. Mater. 29 (48) (2019) 1905273.
[33] Z. Zhao, J. Wu, X. Mu, H. Chen, H.J. Qi, D. Fang, Desolvation induced origami of photocurable polymers by digit light processing, Macromol. Rapid Commun. 38 (13) (2017) 1600625.
[34] D. Han, R.S. Morde, S. Mariani, A.A. La Mattina, E. Vignali, C. Yang, G. Barillaro, H. Lee, 4D printing of a bioinspired microneedle array with backward-facing barbs for enhanced tissue adhesion, Adv. Funct. Mater. 30 (11) (2020) 1909197.
[35] Q. Zhang, X. Kuang, S. Weng, Z. Zhao, H. Chen, D. Fang, H.J. Qi, Rapid volatilization induced mechanically robust shape-morphing structures toward 4D printing, ACS Appl. Mater. Interfaces (2020) 17979–17987, 12(15).
[36] H.M.A. Hamad, Cancer initiatives in Sudan, Ann. Oncol. 17 (2006) viii32–viii36.
[37] C.T. Huynh, M.K. Nguyen, G.Y. Tonga, L. Longé, V.M. Rotello, E. Alsberg, Photocleavable hydrogels for light-triggered siRNA release, Adv. Healthcare Mater 5 (3) (2016) 305–310.
[38] O. Jeon, Y.B. Lee, H. Jeong, S.J. Lee, D. Wells, E. Alsberg, Individual cell-only bioink and photocurable supporting medium for 3D printing and generation of engineered tissues with complex geometries, Mater. Horiz 6 (8) (2019) 1625–1631.
[39] O. Jeon, D.S. Alt, S.M. Ahmed, E. Alsberg, The effect of oxidation on the degradation of photocrosslinkable alginate hydrogels, Biomaterials 33(13) (2012) 3503–3514.
[40] O. Jeon, J.-Y. Shin, R. Marks, M. Hopkins, T.-H. Kim, H.-H. Park, E. Alsberg, Highly elastic and tough interpenetrating polymer network-structured hybrid hydrogels for cyclic mechanical loading-enhanced tissue engineering, Chem. Mater. 29 (19) (2017) 8425–8432.
[41] A.I. Van Den Bulcke, B. Bogdanov, N. De Rooze, E.H. Schacht, M. Cornelissen, H. Berghmans, Structural and rheological properties of methacrylamide modified gelatin hydrogels, Biomacromolecules (2000) 31–38, 1(1).
[42] X. Peng, Y. Li, Q. Zhang, C. Shang, Q.W. Bai, H. Wang, Tough hydrogels with programmable and complex shape deformations by ion dip-dyeing and transfer printing, Adv. Funct. Mater. 26 (25) (2016) 4491–4500.
[43] A. Ding, O. Jeon, R. Tang, Y.B. Lee, S.J. Lee, E. Alsberg, Cell-laden multiple-step and reversible 4D hydrogel actuators to mimic dynamic tissue morphogenesis, Adv, Sci (2021) 2004616.
[44] T.J. Hinton, Q. Jallerat, R.N. Palchesko, J.H. Park, M.S. Grodzicki, H.-J. Shue, M. H. Ramadan, A.R. Hudson, A.W. Feinberg, Three-dimensional printing of complex biological structures by freeform reversible embedding of suspended hydrogels, Sci. Adv 1 (9) (2015) e1500758.
[45] R. Luo, J. Wu, N.D. Dinh, C.H. Chen, Gradient porous elastic hydrogels with shape-memory property and anisotropic responses for programmable locomotion, Adv. Funct. Mater. 25 (47) (2015) 7272–7279.
[46] E. Palleau, D. Morales, M.D. Dickey, O.D. Velev, Reversible patterning and actuation of hydrogels by electrically assisted ionoprinting, Nat. Commun. 4 (1) (2013) 1–7.
[47] J. Liu, W. Xu, Z. Kuang, P. Dong, Y. Yao, H. Wu, A. Liu, F. Ye, Gradient porous PNIPAM-based hydrogel actuators with rapid response and flexibly controllable deformation, J. Mater. Chem. C 8(35) (2020) 12092–12099.
[48] M.M. Ghobashy, G. Bassioni, pH stimuli-responsive poly (acrylamide-co-sodium alginate) hydrogels prepared by γ-radiation for improved compressive strength of concrete, Adv. Polym. Technol. 37 (6) (2018) 2123–2133.
[49] F. Zhang, L. Xiong, Y. Ai, Z. Liang, Q. Liang, Stretchable multiresponsive hydrogel with actuatable, shape memory, and self-healing properties, Adv. Sci. 5 (8) (2018) 1800450.
[50] J. Kim, C. Kim, Y. Song, S.-G. Jeong, T.-S. Kim, C.-S. Lee, Reversible self-bending soft hydrogel microstructures with mechanically optimized designs, Chem. Eng. J. 321 (2017) 384–393.
[51] L. Li, Z.J. Chew, Microactuators: Design and Technology, Smart Sensors and MEMS, Elsevier2018, pp. 313–354.
[52] H.l. Thérien-Aubin, Z.L. Wu, Z. Nie, E. Kumacheva, Multiple shape transformations of composite hydrogel sheets, J. Am. Chem. Soc. 135 (12) (2013) 4834–4839.

[53] K.R. Ryan, M.P. Down, C.E. Banks, Future of additive manufacturing: overview of 4D and 3D printed smart and advanced materials and their applications, Chem. Eng. J. (2020) 126162.
[54] Y.B. Lee, O. Jeon, S.J. Lee, A. Ding, D. Wells, E. Alsberg, Induction of four-dimensional spatiotemporal geometric transformations in high cell density tissues via shape-changing hydrogels, Adv. Func, Mater (2021) 2010104.
[55] T. Rozario, D.W. DeSimone, The extracellular matrix in development and morphogenesis: a dynamic view,, Dev. Biol. 341 (1) (2010) 126–140.
[56] C. Cui, D.-O. Kim, M.Y. Pack, B. Han, L. Han, Y. Sun, L.-H. Han, 4-D printing of self-folding and cell-encapsulating 3-D microstructures as scaffolds for tissue-engineering applications, Biofabrication 12 (4) (2020) 45018.
[57] G. Constante, I. Apsite, H. Alkhamis, M. Dulle, M. Schwarzer, A. Caspari, A. Synytska, S. Salehi, L. Ionov, 4D biofabrication using a combination of 3D printing and melt-electrowriting of shape-morphing polymers, ACS Appl. Mater, Interfaces 13 (11) (2021) 12767–12776.
[58] G.H. Yang, W. Kim, J. Kim, G. Kim, A skeleton muscle model using GelMA-based cell-aligned bioink processed with an electric-field assisted 3D/4D bioprinting, Theranostics 11 (1) (2021) 48.
[59] C. Wang, H. Yue, J. Liu, Q. Zhao, Z. He, K. Li, B. Lu, W. Huang, Y. Wei, Y. Tang, Advanced reconfigurable scaffolds fabricated by 4D printing for treating critical-size bone defects of irregular shapes, Biofabrication 12 (4) (2020) 45025.
[60] Y. Wang, H. Cui, Y. Wang, C. Xu, T.J. Esworthy, S.Y. Hann, M. Boehm, Y.-L. Shen, D. Mei, L.G. Zhang, 4D printed cardiac construct with aligned myofibers and adjustable curvature for myocardial regeneration, ACS Appl. Mater. Interfaces 13 (11) (2021) 12746–12758.
[61] M. Miotto, R.M. Gouveia, A.M. Ionescu, F. Figueiredo, I.W. Hamley, C.J. Connon, 4D corneal tissue engineering: achieving time-dependent tissue self-curvature through localized control of cell actuators, Adv. Funct. Mater. 29 (8) (2019) 1807334.
[62] J.M. Viola, C.M. Porter, A. Gupta, M. Alibekova, L.S. Prahl, A.J. Hughes, Guiding cell network assembly using shape-morphing hydrogels, Adv. Mater. 32 (31) (2020) 2002195.
[63] A.J. Hughes, H. Miyazaki, M.C. Coyle, J. Zhang, M.T. Laurie, D. Chu, Z. Vavrušová, R.A. Schneider, O.D. Klein, Z.J. Gartner, Engineered tissue folding by mechanical compaction of the mesenchyme, Dev. Cell 44 (2) (2018) 165–178.
[64] W. Wei, Y. Ma, X. Yao, W. Zhou, X. Wang, C. Li, J. Lin, Q. He, S. Leptihn, H. Ouyang, Advanced hydrogels for the repair of cartilage defects and regeneration, Bioact. Mater 6 (4) (2021) 998–1011.
[65] O. Jeon, C. Powell, L.D. Solorio, M.D. Krebs, E. Alsberg, Affinity-based growth factor delivery using biodegradable, photocrosslinked heparin-alginate hydrogels, J. Contr. Release 154 (3) (2011) 258–266.
[66] E. Alsberg, K.W. Anderson, A. Albeiruti, R.T. Franceschi, D.J. Mooney, Cell-interactive alginate hydrogels for bone tissue engineering, J. Dent. Res. 80 (11) (2001) 2025–2029.
[67] O. Jeon, D.S. Alt, S.W. Linderman, E. Alsberg, Biochemical and physical signal gradients in hydrogels to control stem cell behavior, Adv. Mater. 25 (44) (2013) 6366–6372.
[68] Z. Tong, L. Jin, J.M. Oliveira, R.L. Reis, Q. Zhong, Z. Mao, C. Gao, Adaptable hydrogel with reversible linkages for regenerative medicine: dynamic mechanical microenvironment for cells, Bioact. Mater 6 (5) (2021) 1375–1387.
[69] A. McMillan, M.K. Nguyen, C.T. Huynh, S.M. Sarett, P. Ge, M. Chetverikova, K. Nguyen, D. Grosh, C.L. Duvall, E. Alsberg, Hydrogel microspheres for spatiotemporally controlled delivery of RNA and silencing gene expression within scaffold-free tissue engineered constructs, Acta Biomater. 124 (2021) 315–326.
[70] R. Tang, K. Umemori, J. Rabin, E. Alsberg, Bifunctional nanoparticle-stabilized hydrogel colloidosomes serve as both extracellular matrix and bioactive factor delivery vehicles, Adv. Ther. 3 (11) (2020) 2000156.
[71] O. Jeon, K. Lee, E. Alsberg, Spatial micropatterning of growth factors in 3D hydrogels for location-specific regulation of cellular behaviors, Small 14 (25) (2018) 1800579.